Applied Catalysis B: Environment and Energy 351 (2024) 123941

Contents lists available at ScienceDirect

Applied Catalysis B: Environment and Energy

journal homepage: www.elsevier.com/locate/apcatb

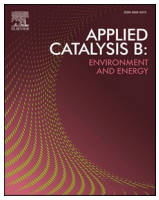

Electrocatalytic urea synthesis from CO_2 and nitrate co-reduction on natural vitamin B_{12} coupled carbon nanotubes

Meiyu Cong [a], Qi Liu [a,*], Dongping Wang [a], Shengjie Hao [a], Zhenze Han [a], Hanen Xu [a], Mingxia Guo [a], Xin Ding [b,*], Yan Gao [a,*]

[a] State Key Laboratory of Fine Chemicals, Dalian University of Technology (DUT), Dalian, Liaoning 116024, China
[b] College of Chemistry and Chemical Engineering, Qingdao University, Qingdao, Shandong 266071, China

ARTICLE INFO

Keywords:
Electrocatalytic urea synthesis
Carbon dioxide
Nitrate
Electrocatalyst
Vitamin B_{12}

ABSTRACT

The synthesis of urea from CO_2 and nitrate co-electrolysis is highly attractive for the sustainable production of nitrogen-containing fertilizers such as urea. However, this process requires electrocatalysts that are not only highly active but also selective. In this study, we present a remarkable approach wherein Vitamin B_{12} is immobilized on the surface of carbon nanotubes to catalyze the co-electroreduction to urea under ambient conditions. This unique hybrid system, incorporating a naturally abundant molecular catalyst, exhibits exceptional selectivity and maintains a constant current density in CO_2-saturated 0.1 M KNO_3. Remarkably, we achieved a Faradaic efficiency (FE) of 26.04% at −0.5 V versus the reversible hydrogen electrode (RHE), resulting in a production yield of 164.04 μg h^{-1} mg^{-1} and an impressive turnover number (TON) reaching up to 830.53 while demonstrating excellent stability and durability over a period of 50 hours. Our experimental findings are further supported by density functional theory (DFT) studies that shed light on the influence exerted by the covalently attached and redox-active benzimidazole unit within Vitamin B_{12} molecule itself when immobilized onto conductive surfaces like carbon nanotubes. This work represents an unprecedented example where naturally abundant vitamin has been successfully immobilized on a conductive surface for achieving highly efficient electroproduction of urea.

1. Introduction

Urea has been a pivotal chemical raw material since its industrial synthesis, serving not only as a nitrogen fertilizer for agricultural crop growth but also as a moisturizer in the pharmaceutical industry for cosmetic products and as a fundamental ingredient in various industrial chemicals.[1] However, the conventional urea production method (Bosch-Meiser) is characterized by high energy consumption, necessitating substantial energy inputs (accounting for 1–2% of global entirety), operating under harsh production conditions (150–200 ∘C, 150–250 bar), involving intricate equipment and processes while emitting significant amounts of CO_2. These factors collectively contribute to an adverse impact on the global carbon cycle.[2,3] Furthermore, the generation of ammonia (NH_3) as a feedstock for industrial urea synthesis heavily relies on the combustion of extensive fossil fuels which poses environmental concerns.[4] Consequently, there exists an urgent imperative to explore sustainable and eco-friendly alternatives that can replace this traditional energy-intensive mode of urea production.

Electrocatalytic synthesis of urea, utilizing electricity derived from renewable green energy sources such as solar and wind power instead of traditional thermal energy, offers a promising pathway for environmentally friendly production. In recent years, there has been increasing attention on the electrocatalytic co-reduction of CO_2 and various N-species (such as nitrogen (N_2)[5–8], nitrate (NO_3^-)[9–16]and nitrite (NO_2^-)[17–21]) under ambient conditions to synthesize urea. Among these species, the highly stable N≡N triple bond energy in N_2(941 kJ mol^{-1}) [22]poses challenges in activation and solubility; whereas nitrate, which contributes to eutrophication in water bodies, possesses a lower N-O bond energy (208 kJ mol^{-1}) [23]that can be readily activated for C-N coupling with CO_2 to produce urea. Therefore, the electrocatalytic co-reduction of CO_2 and nitrate represents a significant pathway towards mitigating greenhouse effects, balancing the nitrogen cycle, and reducing dependence on fossil fuels.

* Corresponding authors.
E-mail addresses: liuqi@dlut.edu.cn (Q. Liu), dingxin@qdu.edu.cn (X. Ding), dr.gaoyan@dlut.edu.cn (Y. Gao).

https://doi.org/10.1016/j.apcatb.2024.123941
Received 3 February 2024; Received in revised form 29 February 2024; Accepted 8 March 2024
Available online 18 March 2024

The synthesis of urea from CO_2 and nitrate has been reported to be thermodynamically spontaneous and theoretically feasible.[24] However, due to the intricate electron-coupled proton transport involving 16 electron transfers and 18 proton transfers, the selectivity of urea generation is significantly lower compared to that of parallel reactions such as nitrate reduction (NRA), CO_2 reduction reaction (CO_2RR), and hydrogen evolution reaction (HER).[25] Furthermore, the C-N coupling during urea formation and subsequent hydrogenation of intermediates require higher energy barriers, thereby substantially inhibiting the kinetics of the reaction.[26] In response to these challenges, researchers have devised innovative catalysts for co-activating CO_2 and NO_3^- in order to achieve higher yields and selectivity in urea production. Among these catalysts , transition metal-nitrogen-carbon (M-N-C) materials , which possess well-defined structure-property relationships that can be precisely tuned and assembled with independent catalytic sites, making them highly efficient for electrocatalytic co-reduction of CO_2 and NO_3^- towards urea production. [23,27]The intricate process of synthesis, however, posed a significant impediment to the advancement of the industry.

VB_{12}, as a naturally occurring molecule, has been reported to be used as a catalyst for CO_2RR [28–30]and nitrate reduction [13]. Moreover, in the field of electrocatalytic research, the unique asymmetric macrocyclic structure of VB_{12} endows the central cobalt site with a unique coordination environment, and the departure of the axial group makes the central cobalt-metal site easier to combine with the reactants, which results in excellent catalytic performance.[11] Therefore, the exceptional natural molecular catalyst VB_{12} exhibits remarkable potential, promising a plethora of favorable outcomes.

Herein, a novel catalyst, VB_{12}-CNTs assembled by Vitamin B_{12} molecular and CNTs, was conveniently synthesized for the electrocatalytic conversion of CO_2 and NO_3^- into urea. The effect of the specific structure of VB_{12} on the electrosynthesis of urea was investigated by comparing it with CoPc-CNTs and CH_3VB_{12}-CNTs electrodes which was assembled by cobalt phthalocyanine and mecobalamine with CNTs differently under identical conditions. To ensure accurate quantification data, nuclear magnetic resonance spectroscopy (NMR) and isotope tracking experiments were employed. Inspired by the advantages of attenuated total reflection Fourier transform infrared spectroscopy (ATR-FTIR), in situ ATR-FTIR was utilized to study the process of electrosynthesis of urea on VB_{12}-CNTs. The catalytic activity source of VB_{12} and the overall reaction pathway for urea synthesis were explored through in situ attenuated total reflection Fourier transform infrared spectroscopy (ATR-FTIR) and theoretical calculations (DFT).

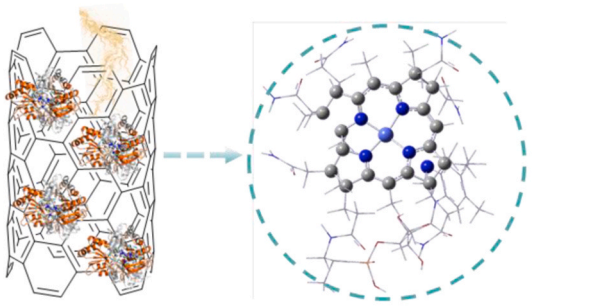

Scheme 1. Electrosynthesis urea by co-reduction CO_2 and NO_3^- on coenzyme-inspired VB_{12}-CNTs.

2. Experimental section

2.1. Chemicals

All chemicals including H_2O_2 (30%), $N_2H_4{\cdot}H_2O$ (50%), $FeCl_3{\cdot}6\ H_2O$, diacetyl oxime, thiosemicarbazide, sulfuric acid, phosphoric acid, potassium nitrate and Vitamin B_{12} were purchased from Sigma-Aldrich Chemical Reagent. potassium nitrate-^{15}N ($K^{15}NO_3$, 99 atom %; ≥ 98.5%), CO_2 gas (99.999%) and Ar gas (99.99%) were purchased from DALIAN NEWRADAR SPECIAL GAS CO., LTD. MWCNTs was bought from Nanjing XFNANO Materials Technology Corporation. The carbon paper (CP) was purchased from Toray Industries in Japan. The d_6-DMSO (99.9 atom% D, Innochem Technology Co., Ltd. Beijing) was adopted as the deuterated solvent. The deionized water used throughout all experiments was purified through a Millipore system. All the reagents were purchased from commercial sources without further purification.

2.2. Preparation of VB_{12}-CNTs/CP electrode

VB_{12}-CNTs/CP electrode was prepared following a previously reported method.[31] 30 mg of purified CNTs were dispersed in 30 mL of DMF with the assistance of sonication for 1 h. Then, 5 mg of VB_{12} dissolved in DMF was added to the MWCNTs suspension followed by 30 min of sonication to obtain a well-mixed suspension. The mixed suspension was further stirred at room temperature for 20 h. Subsequently, the mixture was centrifuged and the precipitate was washed with DMF three times and ethanol twice. Finally, the precipitate was vacuum dried to yield the final VB_{12}-CNT. Catalyst ink was prepared by dispersing 5 mg of catalyst material in a mixture of 50 μL of 0.5 wt% nafion solution and 950 μL of ethanol with the assistance of sonication. The working electrodes were prepared by drop-drying 30 μL of catalyst ink onto carbon paper to cover an area of 0.5 cm^2 and were dried at room temperature overnight. The loading of the catalyst is 0.3 mg/cm^2. The CH_3B_{12}-CNTs and CoPc-CNTs contrast catalysts are consistent with the VB_{12}-CNTs preparation method.

2.3. Characterizations

Transmission electron microscopy (TEM) and energy-dispersive X-ray spectroscopy (EDS) was performed on Tecnai G2 F30. Higher magnification STEM-HAADF imaging and EDX measurements were performed on a double-corrected FEI Themis ZS/TEM at 300 keV accelerating voltage, equipped with a Super-X detector (4 Silicon drift detectors) with a large collection angle of 0.9 rad. Data was processed with FEI Velox software. Before imaging, the probe corrector was carefully calibrated to ensure optimal condition for atomic imaging (defocus C1 and 2- fold astigmatism A1 < 5 nm, 3-fold astigmatism A2 and axial comma B2 < 50 nm, spherical aberration C3 and 4-fold astigmatism A3 and star aberration S3 < 500 nm). 115 mm camera length and 80 pA screen current were setup for HAADF image collecting. VB_{12}-CNTs was imaged by scanning electron microscopy (SEM) on Bruker Smart APEX II. The element composition and states of the materials were performed by X-ray photoelectron spectroscopy (XPS) (Thermo Scientific ESCALAB 250). Specially, the binding energy was standardized concerning to the C 1 s peak at 284.6 eV. Raman spectroscopy was acquired on a DXR Smart using Ar^+ laser excitation. FT-IR spectra (KBr pellets) were collected with a Thermo Electron NEXUS 6700 FT-IR spectrometer. Raman spectrum was observed with an inVia Raman Microscope with a 514 nm (green) diode laser with 1800 l/mm grating. The laser power at the sample position was typically 350 μW with an average spot size of 1 μm in diameter. The Co K-edge X-ray absorption near edge structures (XANES) and extended X-ray absorption fine structure (EXAFS) measurements were carried out on the sample at 21 A X-ray nano-diffraction beamline of Taiwan Photon Source (TPS), National Synchrotron Radiation Research Center (NSRRC). This beamline adopted 4-bounce channel-cut Si (111) monochromator for mono-

beam X-ray nano-diffraction and X-ray absorption spectroscopy. The end-station equipped with three ionization chambers and Lytle/SDD detector after the focusing position of KB mirror for transmission and fluorescence mode X-ray absorption spectroscopy. The photon flux on the sample is range from 1×10^{11} ~3×10^{9} photon/sec for X-ray energy from 6 to 27 keV. The Co content in VB_{12}-CNTs/CP electrode determined by inductively coupled plasma mass spectrometry (ICP-MS) is 1.05×10^{-3} μmol. The turnover numbers (TONs) and turnover frequency (TOF) are calculated as below equation, where $n_{cat.}$ is the total loading amount of catalysts, n_{urea} is the amount of urea, and t is the reaction time.

$$TON_{urea} = \frac{n_{urea}}{n_{cat.}}$$

$$TOF_{urea} = \frac{TON_{urea}}{t}$$

2.4. Electrochemical measurements

The reaction was assessed using a gas-tight, two-compartment cell separated by a Nafion membrane. In a typical test, the catalyst was deposited on carbon paper as the working electrode. Ag/AgCl reference electrode was placed in the cathode chamber. In the anode chamber, a graphite plate was used as counter electrode. Before the experiment, the membrane was boiled in ultrapure water for 1 h, treated in H_2O_2 (5%) aqueous solution at 80 °C for 1 h. Then, the membrane was soaked in 0.5 M H_2SO_4 for 2 h at 80 °C, and subsequently boiled in water for 6 h.

Electrochemical measurements were operated in a standard three-electrode system using a CHI660E electrochemical analyzer (CHI Instruments, Chenhua, Shanghai). Before experiment, the KNO_3 electrolyte (0.1 M, pH = 4.5) in the cathode cell was bubbled with CO_2 for 30 min to ensure that air was excluded in the electrolyte. The entire electrolytic process had sustained for 2 h under each certain potential. All potentials were measured against an Ag/AgCl reference electrode and converted to the RHE reference scale using the equation: E (vs. RHE) = E (vs. Ag/AgCl) + 0.197 V + 0.0591 × pH. The experiments were carried out at room temperature (25 °C). The electrochemical activities of samples were examined by linear sweep voltammetry (LSV) at a scan rate of 5 mV/s. The potential range of the potentiostatic test was − 0.4 ~ − 0.8 V vs RHE, with an interval of 0.1 V. Each potential test for two hours, during which the gas flow rate of CO_2 is 20 mL /min. Potentiostatic test of stability alter the electrolyte every 2 hours.

2.5. Determination of gaseous products

The gas products (H_2, and CO) were detected by an online gas chromatograph equipped with a SP-7890 Plus Shimadzu , thermal conductivity detector (TCD), and flame ionization detector (FID) was used for H_2, and CO quantification. Ultrahigh purity Ar (99.999%) was used as the carrier gas. The volume ratio of gaseous products was calibrated by standard curves from standard gas. The following equation was used to calculate the Faradic efficiency of CO_2 reduction gas products.

$$FE_{(\%)} = \frac{n \times P \times V \times \quad \nu(\mathrm{vol}\%) \times F}{R \times T \times I \quad \times 60(\mathrm{s/min})} \times 100\%$$

where n is the number of electrons for generation of one gas molecule. Both H_2 and CO need 2 electrons, P is the pressure (1.013×10^{5} Pa), V is the gas flow rate measured by a flow meter, ν (vol%) is the volume ratio of H_2 or CO in the GC sampling loop, F is the Faradic constant, R is the ideal gas constant (8.314 m^3 Pa mol^{-1} K^{-1}), T is the reaction temperature (298 K), I is the average current during the sample injection.

2.6. Determination of liquid products

Ammonia: The production of ammonia in the electrolyte was measured using a revised indophenol blue method.[32] 2 mL electrolyte was obtained from the cathodic chamber and mixed with oxidizing solution containing 2 mL NaOH solution (1 M) and 1 mL of NaClO (0.05 M), coloring solution containing salicylic acid (5 wt%), sodium citrate (5 wt%) and 0.2 mL of 1 wt% $Na_2[Fe(NO)(CN)_5]$ for 2 h. The solution was measured with UV-Vis absorption spectrum at 655 nm. The linear curve of the standard concentration was shown in Fig. S17.

NH_4^+ formation rate was calculated using the following equation:

$$NH_4^+ \text{ yield} = C\times V/(m_{cat.}\times t)$$

FE was calculated according to following equation:

$$FE = 8\times C\times V\times F/(18\times Q)$$

Where C is the measured NH_4^+ ion concentration; V is the volume of the cathodic reaction electrolyte; t is the potential applied time; m_{cat} is the loaded quality of catalyst; F is the Faraday constant; and Q is the quantity of applied electricity.

Hydrazine: The hydrazine present in the electrolyte was estimated by the method reported by Watt and Chrisp.[33] A mixture of 5.99 g p-$C_9H_{11}NO$, 30 mL HCI (concentrated,) and 300 mL ethanol was used as a color reagent. Nitrite can affect the color development of hydrazine, and the addition of sulfamic acid can eliminate the effect of nitrite. Mix 2 mL of the solution to be tested and 1 mL sulfamic acid (c=5 mg mL^{-1}), then add 2 mL of color reagent and react at 20 min at room temperature. The UV-Vis absorption spectrum was then acquired at 458 nm, as illustrated in Fig. S20.

FE was calculated according to following equation:

$$FE = 16\times C\times V\times F/(32\times Q)$$

Where 16 refers to the number of electrons that need to be transferred to generate 1 mol of hydrazine; C is the measured N_2H_4 concentration; V is the volume of the cathodic reaction electrolyte; F is the Faraday constant; 32 is the relative molecular mass of hydrazine; and Q is the quantity of applied electricity.

Nitrite: The quantitative determination of nitrite (NO_2^-) is by ion chromatography(IC) method.[34] A series of standard solutions with nitrite concentrations of 0.25, 0.50, 1, 1.5, and 2.0 ppm. A total of 1 mL sample was injected into the injection port. The mobile phase was a mixture of 3.6 mM Na_2CO_3 and $NaHCO_3$, and the NO_2^- peak position was 4.05 min. The model of ion chromatography workstation is Shenghan CIC-D120. The linear fitting curve of standard samples was illustrated in Fig. S16. The content of NO_2^- in the electrolyte was also measured by IC method.

NO_2^- formation rate was calculated using the following equation:

$$NO_2^- \text{ yield} = C\times V/(m_{cat.}\times t)$$

FE was calculated according to following equation:

$$FE = 2\times C\times V\times F/(46\times Q)$$

Urea: The concentration of urea was quantified by the ^1H NMR[35] and diacetylmonoxime method[36].

The Faradaic efficiency and yield for electrocatalytic urea synthesis was obtained by the following equation:

$$\text{urea yield} = C\times V/(m_{cat.}\times t)$$

$$FE = \frac{16 \times F \times C \times \quad V}{60.06 \times Q} \times 100\%$$

where F is the Faraday constant, Q is the electric quantity, C is the concentration of generated urea and V is the volume of the electrolyte, t is the duration of an electrolysis, 16 is the number of electron transfer in

the electrochemical reaction for electro-coupling of CO_2 and nitrate.

For NMR sample preparation, 30 mL of 0.1MKNO_3 containing different standard concentrations of urea was added to an aqueous solution of potassium benzoate as an internal standard. The excess water was removed by spin evaporation, cooled to room temperature then 1.0 mL of deuterated methylsulfoxide was added to the flask and sonicated for one hour to fully dissolve it, then the liquid was transferred to the NMR tube. The NMR test was conducted under the hydrogen spectroscopy mode with a scanning circle of 320 times. The formation rate of urea was averaged by the time, and the presented urea formation rate was the average value within the time frame of the tests. The linear curve of the standard concentration was shown in Figure S19.

Diacetyl oxime detection urea method is as follows: First, 1 mL aliquot of the solution was removed from the electrochemical reaction vessel. Then 2 mL acid-ferric solution (100 mL concentrated phosphoric acid, 300 mL concentrated sulfuric acid, 600 mL deionized water and 100 mg ferric chloride) and 1 mL diacetylmonoxime (DAMO)-thiosemicarbazide (TSC) solution (5 g DAMO and 100 mg TSC were dissolved in 1000 mL deionized water) were added. Then the solution was heated to 100 °C and maintained for 20 min. After cooling to room temperature, the absorbance was acquired at 525 nm using a UV–Vis spectrophotometer (Shimadzu UV-1900i). The linear curve of the standard concentration was shown in Figure S18.

2.7. The experiments of the ^{15}N Isotopic of urea

The ^{15}N isotopic labeled experiment were performed using the $K^{15}NO_3$ isotope with the ^{15}N (99.99%) to certify the NO_3^- origination of urea. Before the electrochemical reduction, 30 mL 0.1 M $K^{15}NO_3$ pretreated electrolytewas saturated with CO_2 for 30 min. After electrolysis, the electrolyte was concentrated by a rotatory evaporator, resulting in the formation of ^{15}N-urea. Then the products were dissolved in 1.0 mL of dimethylsulfoxide-d6 (99.9%, Sigma Aldrich), followed by analyzed with 1 H nuclear magnetic resonance (^1H NMR) spectrometer (Bruker AVANCE III 600).

2.8. ATR-FTIR measurements

The electrolyte in the chamber of customized cell during the reaction. ATR-FTIR in situ testing was performed using an INVENIO R FT-IR (Bruker) spectrometer equipped with an MCT detector; all spectra are expressed in transmittance. The spectral resolution is 4 cm^{-1}, and the scan time for each curve is 10 seconds. The scan rate was 20 kHz.

2.9. Computational details

The density functional theory is performed in a plane wave pseudopotential implementation, employing Vienna Ab-initio Simulation Package (VASP). [37,38]All the calculations are carried out within the pseudopotential approximation whereby the electrons are described in the generalized gradient approximation (GGA)-PBE exchange-correlation correlation functional[39]. The empirical D2 approach[40] as implemented in VASP is employed to describe the van der Waals interactions. Dipole corrections[40] are also considered because in our models, the absorbents are only adsorbed on one side of the slab with periodic boundaries. The catalyst, VB_{12}-CNT structured carbon composite, is modeled on a super cell more than 20 Å ×20 Å in a-b plane to prevent strong coupling between the individual absorbed VB_{12} molecules and is separated by at least 20 Å vacuum regions to ensure decoupling between next slabs. One VB_{12} molecule is permitted to be adsorbed on CNTs. For the large dimension of the super cell, 1×1 × 1 (gamma point) Monkhorst-Pack k-point sampling was used. The electron wave function is expanded using plane waves with an energy cutoff of 550 eV. Geometric optimization is performed until energy and forces are less than 10^{-4} eV or 0.02 eV/Å.

3. Results

3.1. Structural characterization

The VB_{12}-CNTs composite was synthesized via a self-assembly pathway, where VB_{12} and CNTs were tightly bound through π-π interactions under ultrasonic treatment in N, N-dimethylformamide (DMF) solution.[41–43] After centrifugal drying, the resulting black powder was identified as CNTs-loading VB_{12} molecular catalyst. Scanning electron microscopy (SEM) images of VB_{12}-CNTs (Fig. S1) revealed a smooth surface without any noticeable aggregation of VB_{12} particles on the CNTs surface. This observation was further confirmed by transmission electron microscopy (TEM) and high-resolution TEM (HRTEM) images shown in Fig. S2(A) and (B). In the enlarged spherical aberration corrected high angle annular dark field scanning transmission electron microscope (HADDF-STEM) image, as shown in Fig. S2(C), the interior of CNTs remained smooth while the outer surface exhibited attached VB_{12} molecules with bright white areas corresponding to cobalt atoms, which are more clearly depicted in Fig. 1(A). Notably, numerous Ångstrom-sized bright spots were evenly distributed on the CNTs' surface and predominantly appeared as individual occurrences marked by yellow circles. The significant brightness contrast observed for metal atoms in dark field imaging[44] indicated that the dispersed form of VB_{12} molecules on the CNT surface consisted of individual molecules rather than clusters. Furthermore, HRTEM image of VB_{12}-CNTs in Fig. 1(B) and corresponding energy-dispersive X-ray spectroscopy (EDS) element mapping analysis presented in Fig. 1(C) demonstrated homogeneous dispersion patterns for Co, N, O, and P elements constituting the loaded VB_{12} molecules on carbon nanotubes' external surface, which was aligned well with our design expectations for catalyst synthesis.

In order to accurately further characterize the elemental state and atomic coordination environment of the Co atom in VB_{12}-CNTs, synchrotron radiation X-ray absorption spectroscopy (XAS) was conducted. The X-ray absorption near-edge structure (XANES) profiles (Fig. 1D) magnified the normalized absorption edge of the Co K-edge in VB12-CNTs, with reference standards including Co foil(N), CoO(II), and Cobalt(II) phthalocyanine (CoPc). After a meticulous analysis and fitting of the spectra, the energy value (E_0) was derived as presented in Table S1, leading to the conclusion that the oxidation states for CoO powder, pristine CoPc, VB12-CNTs, and pristine Co foil are 2+, 2+, 3+, and 0 respectively. This unequivocally demonstrates that the VB_{12} molecules immobilized on the surface of CNTs remained structurally unaltered while preserving their original molecular configuration.

Furthermore, within XANES spectra's pre-edge region spanning from 7700 to 7722 eV (depicted in Fig. 1(A)'s inset), a robust characteristic peak at approximately 7710 eV is observed for VB_{12}-CNTs while exhibiting a slight rightward shift for CoO powder, both indicating six-coordinated octahedral species. In contrast, another distinct peak at around 7717 eV prominently appears for pristine CoPc but is absent in both CoO powder and VB_{12}-CNTs. It should be emphasized that pristine CoPc consists of a four-coordinated square-planar structure. As reported, the six- and five-coordinated VB_{12} species yielded strong XANES peaks at 7710 eV, but the four-coordinated VB_{12} species yielded a strong peak at 7714 eV. [45]Thus, the central Co in VB_{12}-CNTs is most likely to be a six-coordinated structure, this phenomenon indicates that the surface coupling process between VB_{12} molecules and CNTs does not change the initial molecules' structure. Extended X-ray absorption fine structure (EXAFS) was performed on the Co K-edge spectra for further the Co coordination number issue in VB_{12}-CNTs, which yields precise metal–ligand distances and the coordination number of the central Co in VB_{12}-CNTs. As shown in Fig. 1(E), Fourier transformation of k^3-weighted Co K-edge EXAFS data for VB_{12}-CNTs shows that Co-N is the major coordination bond are attached to the central corrin ring in the VB_{12} molecule, and there are no Co-O or metal Co-Co bond. The structural parameters obtained from curve fitting to these spectra are listed in Table S2, which clearly suggests that Co atom in VB12-CNTs has a

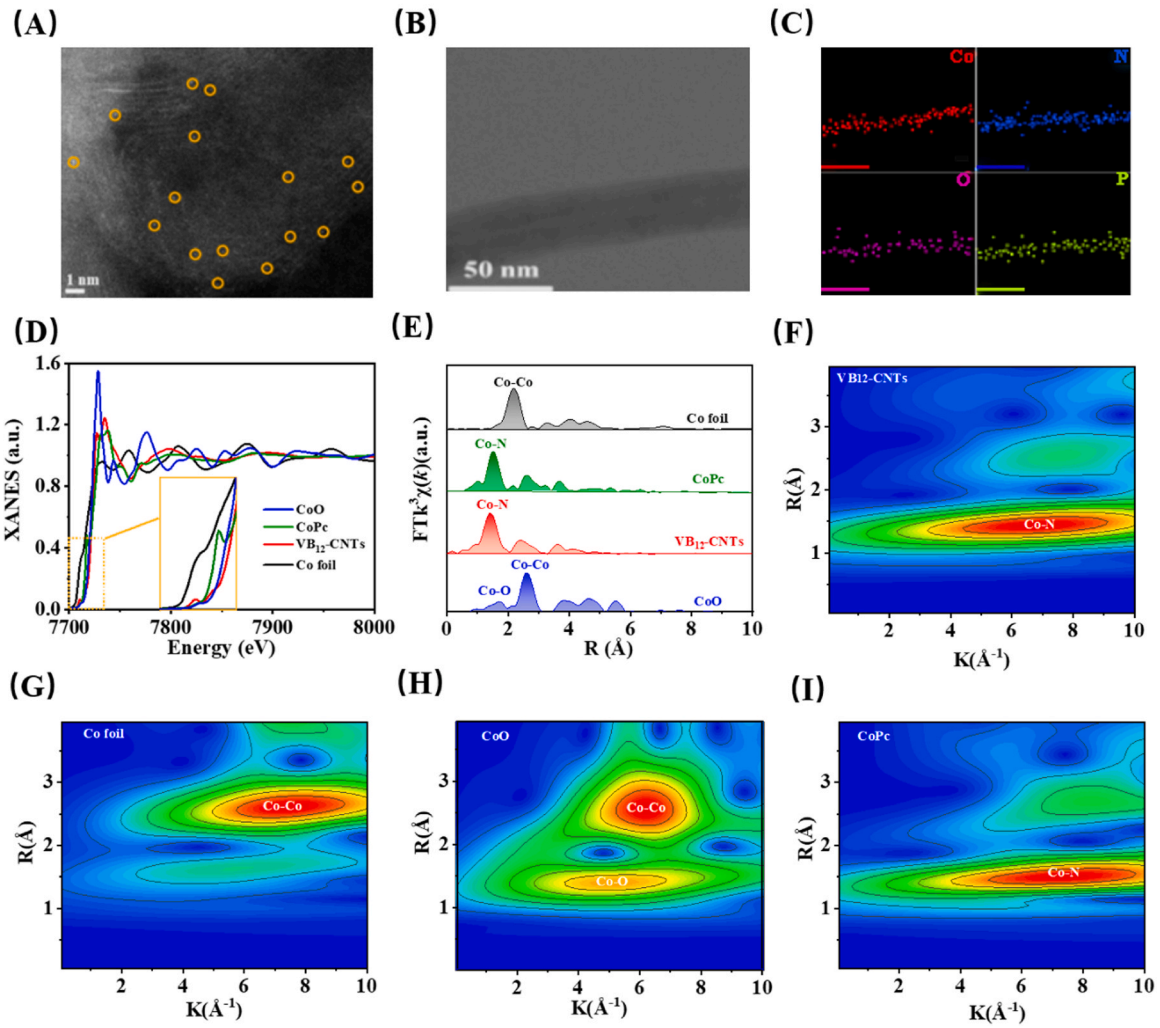

Fig. 1. (A) Aberration-corrected HAADF- STEM image of VB_{12}-CNTs. (B) HRTEM image of VB_{12}-CNTs and corresponding EDS elemental mapping images of Co, N, O and P elements in (C). (D) XANES spectra of CoO powder, pristine CoPc, VB_{12}-CNTs, and Co foil. (E) Fourier transforms of k^3-weighted EXAFS data at the Co K-edge for four samples. (F-I) WT-EXAFS of VB_{12}-CNTs, Co foil, CoO and CoPc.

coordination number of 6. [46]Therefore, based on the XANES and EXAFS results, VB_{12}-CNTs prepared by in situ assembly at room temperature maintain the initial conformation of the VB_{12} molecule and are not subject to adjustment, in line with the HAADF- STEM observation. Additionally, to explain the metal coordination path, wavelet transform (WT)-EXAFS was also conducted in *k*-space resolution (Fig. 2(F-I)). Distinguished from the Co-Co or Co-N bonding in Co foil and pristine CoPc, the intensity center of Co-N in VB12-CNTs were at ~1.4 $Å^{-1}$, matching the coordination numbers from least-squares EXAFS fitting (Table S1). The best fitting results (Fig. S3-4) also demonstrated the VB_{12} molecules on the surface of CNTs maintain a six-coordinated conformation, as we expected.

In order to further investigate the valence changes of cobalt atoms in the center corrin ring of VB_{12} molecules coupled on the surface of CNTs, x-ray photoelectron spectroscopy (XPS) measurements were carried out for probing the surface chemical features of VB_{12} and VB_{12}-CNTs. The surface chemical composition of three samples as CNTs, VB_{12}-CNTs and VB_{12} were identified in a wide energy range shown in Fig. S5, and the elements C, N, O, Co and P were presented on the surface. Elemental scan spectra for Co 2*p*, C 1 *s*, N 1 *s*, O 1 *s* and P 2*p* confirmed the composition of VB_{12} and VB12-CNTs (Fig.S6-S8). The binding energy of Co $2p_{3/2}$ and Co $2p_{1/2}$ can be observed at 781.0 eV and 796.1 eV, respectively. As shown in Fig. S7(A and C), compared with VB_{12}, the C 1 *s* signals of VB_{12}-CNTs were slightly shifted to low binding energy: C-H (284.6 eV), C-C (285.2 eV) and C═O (286.6 eV)[47], respectively. It indicated a strong interaction between VB_{12} and CNTs.[29] Fig. S7(B and D) showed that the N 1 *s* peaks of VB_{12} were deconvoluted to pyridinic N (398.3 eV) and amino N (399.1 eV)[48], respectively. Compared with VB_{12}, the N 1 *s* signals of VB_{12}-CNTs were slightly shifted to high binding energy demonstrating that the strong interaction between VB_{12} and CNTs. Moreover, this shift of elemental peaks also occurs in O 1 *s* and P 2*p*, again demonstrating the tight binding of VB_{12} molecules on the surface of CNTs. The XRD spectra in Fig. S9 of VB_{12}-CNTs showed that CNTs coupled with VB_{12} molecules not only had the characteristic crystal shape of CNTs (26°), but also the characteristic peaks of VB_{12} molecules appeared in the small peak energy range (5–10°), compared to pure VB_{12} molecules and CNTs. Raman spectra of the samples also revealed that the peak intensity ratio of D to G (I_D/I_G) decreased from 0.65 of VB_{12}-CNTs to 0.67 of pure CNTs, indicating the π-π interaction between CNTs and VB_{12} strengthened the conjugation after modifying VB_{12} which was compatible with XPS results in Fig. S10. The above characterization results show that VB_{12} molecules are successfully coupled to the surface of CNTs, which provides a basis for subsequent electrochemical tests.

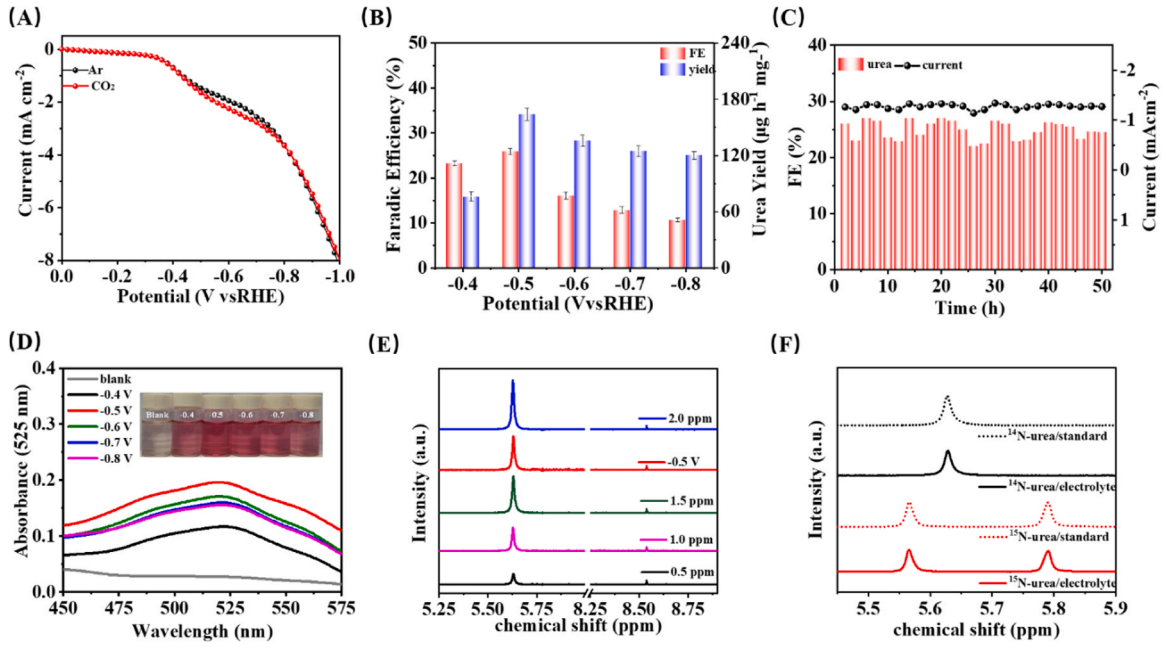

Fig. 2. (A) LSV curves of the VB_{12}-CNTs in 0.1 M KNO_3 electrolyte with Ar or CO_2 feeding gas. (B) Dependence of urea yield and FE on the applied potentials for 2 h reaction. (C) Stability test of the VB_{12}-CNTs at −0.50 V (vs. RHE). (D) UV-Vis spectra of the electrolyte (0.1 M KNO_3) of VB_{12}-CNTs after charging at different potentials for 2 h with CO_2 by using diacetyl monoxime method. (E) The ^{1}H NMR spectra for standard ^{14}N-urea, potassium benzoate as internal label. (F) The ^{1}H NMR spectra for standard urea sample and direct urea product of VB_{12}-CNTs at −0.5 V vs RHE for isotope labeling measurements.

3.2. Electrocatalytic urea synthesis

With the successful synthesis of VB_{12}-CNTs molecular catalyst, the electrocatalytic urea synthesis was conducted on a typical three-electrode H-cell reactor at room temperature and atmospheric pressure. The as-employed electrolyte (0.1 M KNO_3) was saturated with CO_2 bubbling, which was continuously streamed to the cathode during the chronoamperometry tests. The urea products were quantitatively determined by the diacetyl monoxime standard curve method according to the characteristic absorption at 525 nm in the UV–vis spectra[11] (Fig. S18). Firstly, the linear sweep voltammetry (LSV) tests were performed initially from 0.0 to −1.0 V vs. RHE with saturated CO_2 or Ar and KNO_3 electrolyte to evaluate the electrochemical response of VB_{12}-CNTs towards urea. Compared to that in the Ar/KNO_3 with CO_2/KNO_3 system, the VB_{12}-CNTs heterostructures exhibited an enhanced current density from −0.4 to −0.8 V vs. RHE in CO_2-saturated 0.1 M KNO_3 electrolyte (Fig. 2(A)), indicating the occurrence of efficient urea electrosynthesis reaction. [20,21,25] Constant potential tests with electrolysis times of 2 h at intervals of 0.1 V were performed over a potential range of −0.4 V to −0.8 V vs. RHE according to the potential range provided by LSV for urea synthesis. The Faraday efficiencies (FE) and yields of urea synthesized by electrolysis at each potential are summarized in Fig. 2(B) based on the quantification of urea performed by the diacetoxime method in Fig. 2(D). As can be seen from the Fig. 2(B), the FE and yield of urea synthesis at the VB12-CNTs electrode showed an obvious volcano type trend of increasing and then decreasing in the selected potential range, and the optimal potential was −0.5 V vs. RHE, and the FE and yield of urea synthesis obtained at this potential were 26.04% and 164.04 μg h^{-1} mg^{-1}, respectively. It was thus shown that the synthesis of urea by the co-electrical reduction of CO_2 and NO_3^- mainly occurred in the low negative potential region, and with the increase of more negative potential, the electroreduction reaction was further inclined to other parallel reactions, which could inhibit the urea synthesis. Surprisingly, the synthesized products did not contain any carbon-containing species when VB_{12}-CNTs were used as co-reduction electrodes, indicating that the catalyst could effectively inhibit the electrocatalytic reduction reaction of CO_2, which was rather favorable for urea synthesis.

Of course, a good electrocatalyst necessitates not only efficient product selectivity but also exceptional durability. Hence, the same VB_{12}/CNTs electrode was employed as the working electrode, and its current density and FE of synthesized urea remained unaltered even after 50 cycle tests, thereby ensuring an exemplary service life. Furthermore, it has been reported that the concentration of nitrite produced during co-electrolysis impacts the UV color development of urea, leading to erroneous positives or diminished urea concentrations; however, NMR quantitative testing of urea remains unaffected.[49] Consequently, NMR quantitative testing was conducted subsequent to electrolyte concentration, yielding nearly identical results to UV quantification and thus validating the reliability of the obtained urea quantitative data. In order to ascertain the source of reactants for synthesizing urea in the final product, isotope tracking experiments utilizing ^{15}N were employed for estimation purposes. As depicted in Fig. 2(F), when $K^{15}NO_3$ served as the nitrogen source in an electrolyte with saturated CO_2 utilization, there was consistent production of target standard ^{15}N-urea concentration without significant deviation from that achieved using $K^{14}NO_3$ as an electrolyte. The outcomes derived from NMR tests ensured accuracy in quantifying urea while demonstrating that NO_3^- within the electrolyte serves as a nitrogen source for producing urea. Additional control experiments (Fig.S22) revealed no production of urea by VB_{12}-CNTs electrodes in absence of CO_2 presence and similarly no synthesis occurred when NH_4^+ was present within an electrolytic environment containing saturated CO_2; this suggests that both CO_2 and NO_3^- are essential prerequisites for electrosynthesis of urea.

3.3. Activity analysis

The synthesis efficiency of the products over molecular-catalyst is an important indicator for evaluating their catalytic performance, including the turnover number (TON) and turnover frequency (TOF) [50]. According to the Co content in VB_{12}-CNTs electrode determined by inductively coupled plasma mass spectrometry (ICP-MS), the corresponding total TON and TOF of urea generation are calculated to be 830.53 and 0.11 s^{-1}, respectively, indicating that VB_{12}-CNTs electrode

by facile assembly way had efficient urea electrosynthesis activity. In order to investigate the source of catalytic activity of VB_{12} molecules, CH_3VB_{12} and CoPc with similar structures were used for electrode preparation utilizing the same assembly and used in electrocatalytic synthesis of urea experiments, and the obtained urea FEs and yields were summarized in Fig. 3(A). The results showed that both CH_3VB_{12} with axial groups that are not easily dissociated and CoPc with symmetric Co-N4 structure are not favorable for urea synthesis, suggesting that the intrinsically optimized catalytic sites of VB_{12} molecules in electrolytic environments are the key to the efficient synthesis of urea. Moreover, the LSV curves under the same electrolytic environment also indicated that the VB_{12}-CNTs possessed the highest current density for urea synthesis, shown in Fig. S23. Experimentally, advanced operando ATR-FTIR measurements were conducted on VB_{12}-CNTs to validate the C–N coupling mechanism. The infrared signals are collected from 1000 to 4000 cm^{-1} during negative scan from −0.4 to −0.8 V vs.RHE in Fig. 3 (B). For the range from 1000 to 1800 cm^{-1}, infrared bands are probed at 1575 and 1140 cm^{-1}, which are assignable to the bending mode and rocking mode of $–NH_2$ in urea. [51]Apart from the infrared bands of $–NH_2$, the stretching mode of C–N can be observed at 1425 cm^{-1}. [52, 53]The operando ATR-FTIR results of from 3000 to 3600 cm^{-1} confirm the emergence of H–N–H stretching mode and N–H bending mode at 3296, and 3389 cm^{-1}[51], respectively. The intensities of these characteristic peaks also showed significant variations with increasing applied potential, most notably the highest intensity at −0.5 V vs.RHE, which is consistent with the trend of FE and yield changes in urea electrochemical synthesis experiments. Evidenced by the operando ATR-FTIR results, the C–N coupling is successfully realized for subsequent urea synthesis. These results explicitly justify the presence of CO_2NH_2 intermediate and the rate-determining step is also proved to be the protonation of $*CO_2N$ into $*CO_2NH_2$, in line with the preceding theoretical analysis.

3.4. DFT calculation

To unravel the fundamental original activity of the VB_{12} molecules' natural optimized structure, density functional theory (DFT) calculations are conducted. The adsorption of NO_3^- on the surface of the catalytic sites is the first step in the electrocatalytic synthesis of urea from urea, so the nitrate adsorption capacity of the cobalt sites was calculated under different possible coordination environments. In light of the free-energy diagram of the lowest energy pathway as profiled in inset of Fig. 3(C), the urea production initiates from thermodynamically spontaneous reduction of NO_3^- (HNO_3) to $*NO_2$ intermediate on four coordinated VB_{12} molecules which were anchored on surface of CNTs in 0.1 M KNO_3 electrolyte saturated bubbled CO_2 with an adsorption free energy of −0.49 eV. However, the nitrate adsorption on the Co site of five-coordinated structure named as corrin-DMB or coordination-saturated CH_3VB_{12} were both endothermic and not conducive to further urea synthesis. Thus, complete pathway calculations for the

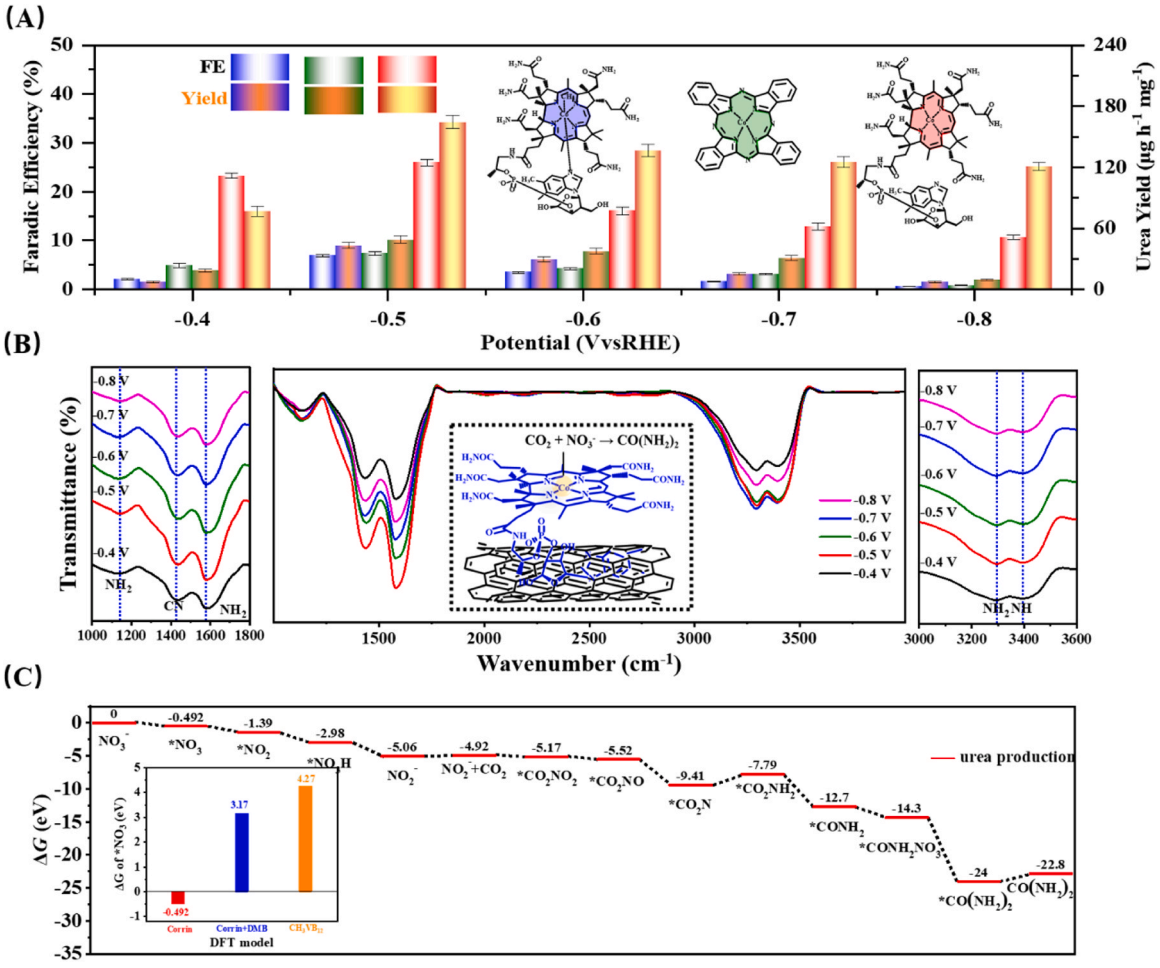

Fig. 3. (A) The FE of urea and corresponding yield rate on CH_3VB_{12}-CNTs (blue), CoPc-CNTs (green) and VB_{12}-CNTs (red) at various applied potentials (vs.RHE) for 2 h of electrocatalysis. (B) In situ electrochemical infrared spectroscopy measurements for VB_{12}-CNTs during the electrocoupling of NO_3^- and CO_2. (C) Free-energy diagram for urea production on the single Co site of VB_{12}-CNTs at 0 V vs. RHE. The internal diagram is the adsorption energy of NO_3^- on the cobalt sites of VB_{12} molecules with different structures.

preparation of urea by electrocatalytic co-reduction of CO_2 and NO_3^- were performed on the simplified corrin configuration, shown in Fig. 3 (C), and the intermediate configurations for each step are shown in Fig. S27. In Fig. 3(C), the free energy of the intermediates in each step of urea synthesis is spontaneously exothermic, including the formation of $*CO_2NH_2$ in the decisive step, with a free energy change of 1.62 eV. The overall reaction pathway shows a kinetically feasible downhill trend, suggesting that VB_{12} molecules have naturally optimized catalytic sites for electrocatalytic urea synthesis under ambient condition.

4. Conclusion

In summary, a novel electrocatalyst, VB_{12}-CNTs, was synthesized using a facile assembly method for efficient urea production. This synthesis strategy combined the catalytic performance of Co-N_4 in VB_{12} with the high conductivity of CNTs. Under CO_2-saturated 0.1 M KNO_3 electrolyte, the VB_{12}-CNTs electrode exhibited remarkable electrochemical performance with a high faradaic efficiency (FE) for urea production at 26.02% and a corresponding yield of 164.04 μg^{-1} h^{-1} mg^{-1} at −0.5 V (vs RHE). Moreover, long-term cycling experiments over 50 hours demonstrated that the prepared VB_{12}-CNTs electrode possessed superior durability in electrocatalytic urea synthesis compared to most existing catalyst electrodes. Additionally, through in situ ATR-FTIR technique analysis, it was confirmed that C-N coupling occurred on the surface of the VB_{12}-CNTs catalyst during urea synthesis reactions. Furthermore, DFT calculations revealed that hydrogenation of nitrogen after complete deoxygenation via C-N coupling served as the rate-limiting step in overall urea electrosynthesis process. This study will inspire further exploration into naturally abundant substances with catalytic activity for transforming waste small molecules into valuable chemical products.

CRediT authorship contribution statement

Zhenze Han: Validation, Data curation. **Meiyu Cong:** Writing – original draft, Formal analysis. **Qi Liu:** Software. **Dongping Wang:** Writing – review & editing, Methodology. **Shengjie Hao:** Validation, Data curation. **Yan Gao:** Writing – review & editing, Funding acquisition. **xin ding:** Writing – review & editing, Supervision. **Hanen Xu:** Validation, Data curation. **Mingxia Guo:** Validation, Data curation.

Declaration of Competing Interest

The authors declare that they have no known competing financial interests or personal relationships that could have appeared to influence the work reported in this paper.

Data Availability

Data will be made available on request.

Acknowledgements

All authors contributed equally to this work. This study was supported by the National Natural Science Foundation of China (Grant Nos. 22278055 and 22109078).

Appendix A. Supporting information

Supplementary data associated with this article can be found in the online version at doi:10.1016/j.apcatb.2024.123941.

References

[1] E.S. Wibowo, B.-D. Park, V. Causin, Recent advances in urea–formaldehyde resins: converting crystalline thermosetting polymers back to amorphous ones, Polym. Rev. 62 (2021) 722–756.
[2] J. Li, Y. Zhang, K. Kuruvinashetti, N. Kornienko, Construction of C–N bonds from small-molecule precursors through heterogeneous electrocatalysis, Nat. Rev. Chem. 6 (2022) 303–319.
[3] R. Xia, S. Overa, F. Jiao, Emerging electrochemical processes to decarbonize the chemical industry, JACS Au 2 (2022) 1054–1070.
[4] C.J.M. van der Ham, M.T.M. Koper, D.G.H. Hetterscheid, Challenges in reduction of dinitrogen by proton and electron transfer, Chem. Soc. Rev. 43 (2014) 5183–5191.
[5] W. Wu, Y. Yang, Y. Wang, T. Lu, Q. Dong, J. Zhao, J. Niu, Q. Liu, Z. Hao, S. Song, Boosting electrosynthesis of urea from N2 and CO2 by defective Cu-Bi, Chem. Catal. 2 (2022) 3225–3238.
[6] C. Chen, X. Zhu, X. Wen, Y. Zhou, L. Zhou, H. Li, L. Tao, Q. Li, S. Du, T. Liu, D. Yan, C. Xie, Y. Zou, Y. Wang, R. Chen, J. Huo, Y. Li, J. Cheng, H. Su, X. Zhao, W. Cheng, Q. Liu, H. Lin, J. Luo, J. Chen, M. Dong, K. Cheng, C. Li, S. Wang, Coupling N2 and CO2 in H2O to synthesize urea under ambient conditions, Nat. Chem. 12 (2020) 717–724.
[7] M. Yuan, J. Chen, Y. Bai, Z. Liu, J. Zhang, T. Zhao, Q. Shi, S. Li, X. Wang, G. Zhang, Electrochemical C–N coupling with perovskite hybrids toward efficient urea synthesis, Chem. Sci. 12 (2021) 6048–6058.
[8] C. Zhu, Y. Geng, X. Yao, G. Zhu, Z. Su, M. Zhang, Fascinating electrocatalysts with dispersed Di-metals in MN3-M'N4 moiety as two active sites separately for N2 and CO2 reduction reactions and jointly for C□N coupling and urea production, Small Methods 7 (2023) 2201331.
[9] N. Meng, X. Ma, C. Wang, Y. Wang, R. Yang, J. Shao, Y. Huang, Y. Xu, B. Zhang, Y. Yu, Oxide-derived core–shell Cu@Zn nanowires for urea electrosynthesis from carbon dioxide and nitrate in water, ACS Nano 16 (2022) 9095–9104.
[10] C.D. Lv, C. Lee, L.X. Zhong, H.J. Liu, J.W. Liu, L. Yang, C.S. Yan, W. Yu, H.H. Hng, Z.M. Qi, L. Song, S.Z. Li, K.P. Loh, Q.Y. Yan, G.H. Yu, A Defect Engineered Electrocatalyst that Promotes High-Efficiency Urea Synthesis under Ambient Conditions, Acs Nano 16 (2022) 8213–8222.
[11] L. Chade, Z. Lixiang, L. Hengjie, F. Zhiwei, Y. Chunshuang, C. Mengxin, K. Yi, L. Carmen, L. Daobin, L. Shuzhou, L. Jiawei, S. Li, C. Gang, Y. Qingyu, Y. Guihua, Selective electrocatalytic synthesis of urea with nitrate and carbon dioxide, Nat. Sustain 4 (2021) 868–876.
[12] X. Zhang, X. Zhu, S. Bo, C. Chen, M. Qiu, X. Wei, N. He, C. Xie, W. Chen, J. Zheng, P. Chen, S.P. Jiang, Y. Li, Q. Liu, S. Wang, Identifying and tailoring C–N coupling site for efficient urea synthesis over diatomic Fe–Ni catalyst, Nat. Commun. 13 (2022) 5337.
[13] X. Wei, X. Wen, Y. Liu, C. Chen, C. Xie, D. Wang, M. Qiu, N. He, P. Zhou, W. Chen, J. Cheng, H. Lin, J. Jia, X.-Z. Fu, S. Wang, Oxygen vacancy-mediated selective C–N coupling toward electrocatalytic urea synthesis, J. Am. Chem. Soc. 144 (2022) 11530–11535.
[14] X. Wei, Y. Liu, X. Zhu, S. Bo, L. Xiao, C. Chen, T.T.T. Nga, Y. He, M. Qiu, C. Xie, D. Wang, Q. Liu, F. Dong, C.-L. Dong, X.-Z. Fu, S. Wang, Dynamic reconstitution between copper single atoms and clusters for electrocatalytic urea synthesis, Adv. Mater. 35 (2023) 2300020.
[15] X. Tu, X. Zhu, S. Bo, X. Zhang, R. Miao, G. Wen, C. Chen, J. Li, Y. Zhou, Q. Liu, D. Chen, H. Shao, D. Yan, Y. Li, J. Jia, S. Wang, A universal approach for sustainable urea synthesis via intermediate assembly at the electrode/electrolyte interface, Angew. Chem., Int. Ed. 63 (2023) e202317087.
[16] M. Qiu, X. Zhu, S. Bo, K. Cheng, N. He, K. Gu, D. Song, C. Chen, X. Wei, D. Wang, Y. Liu, S. Li, X. Tu, Y. Li, Q. Liu, C. Li, S. Wang, Boosting electrocatalytic urea production via promoting asymmetric C–N coupling, CCS Chem. 5 (2023) 2617–2627.
[17] N. Meng, Y. Huang, Y. Liu, Y. Yu, B. Zhang, Electrosynthesis of urea from nitrite and CO2 over oxygen vacancy-rich ZnO porous nanosheets, Cell Rep. Phys. Sci. 2 (2021) 100378.
[18] D. Zhang, Y. Xue, X. Zheng, C. Zhang, Y. Li, Multi-heterointerfaces for selective and efficient urea production, Natl. Sci. Rev. 10 (2023) nwac209.
[19] M. Velpandian, V. Dhongde, K. Singh, P. Gupta, D. Sarma, A. Mahata, S. Basu, Understanding urea electro synthesis using layered perovskite $NdBa_{0.25}Sr_{0.75}Co_2O_{5+\delta}$ cathode material, Chem. Eng. Res. Des. 198 (2023) 1–13.
[20] S. Liu, S. Yin, Z. Wang, Y. Xu, X. Li, L. Wang, H. Wang, AuCu nanofibers for electrosynthesis of urea from carbon dioxide and nitrite, Cell Rep. Phys. Sci. 3 (2022) 100869.
[21] P. Li, Q. Zhu, J. Liu, T. Wu, X. Song, Q. Meng, X. Kang, X. Sun, B. Han, Efficient C–N coupling for urea electrosynthesis on defective Co_3O_4 with dual-functional sites, Chem. Sci. (2024) (Advance Article).
[22] D. Jiao, Y. Dong, X. Cui, Q. Cai, C.R. Cabrera, J. Zhao, Z. Chen, Boosting the efficiency of urea synthesis via cooperative electroreduction of N_2 and CO_2 on MoP, J. Mater. Chem. A 11 (2023) 232–240.
[23] J. Leverett, T. Tran-Phu, J.A. Yuwono, P. Kumar, C. Kim, Q. Zhai, C. Han, J. Qu, J. Cairney, A.N. Simonov, R.K. Hocking, L. Dai, R. Daiyan, R. Amal, Tuning the Coordination Structure of Cu-N-C Single Atom Catalysts for Simultaneous Electrochemical Reduction of CO_2 and NO_3^- to Urea, Adv. Energy Mater. 12 (2022) 2201500.
[24] M. Shibata, K. Yoshida, N. Furuya, Electrochemical synthesis of urea at gas-diffusion electrodes: IV. Simultaneous reduction of carbon dioxide and nitrate ions with various metal Catalysts, J. Electrochem. Soc. 145 (1998) 2348.
[25] W. Hua, J. Yong, L. Sijun, G. Fenglin, L. Xiaorui, J. Yimin, L. Wei, S. Wei, H. Rongxing, L. Ming, Realizing efficient C-N coupling via electrochemical co-

reduction of CO_2 and NO_3^- on AuPd nanoalloy to form urea: Key C-N coupling intermediates, Appl. Catal., B 318 (2022) 121819.
[26] Z. Jingui, X. Shaohan, S. Jie, Z. Jinxing, S. Lingzhi, P. Xun, L. Lina, Z. Guohua, Boosting efficient C-N bonding toward photoelectrocatalytic urea synthesis from CO2 and nitrate via close Cu/Ti bimetallic sites, Appl. Catal., B 338 (2023) 123056.
[27] Q. Zhao, X. Lu, Y. Wang, S. Zhu, Y. Liu, F. Xiao, S.X. Dou, W.-H. Lai, M. Shao, Sustainable and high-rate electrosynthesis of nitrogen fertilizer, Angew. Chem., Int. Ed. 62 (2023) e202307123.
[28] C. Jia, K. Ching, P.V. Kumar, C. Zhao, N. Kumar, X. Chen, B. Das, Vitamin B12 on graphene for highly efficient CO2 electroreduction, ACS Appl. Mater. Interfaces 12 (2020) 41288–41293.
[29] N. Saravanan, M. Balamurugan, K.S. Shalini Devi, K.T. Nam, A. Senthil, Vitamin B12-immobilized graphene oxide for efficient electrocatalytic carbon dioxide reduction reaction, ChemSusChem 13 (2020) 5620–5624.
[30] S. Xin, Y. Hu, W. Fang, J. Dang, Y. Wu, M. Li, W. Cui, Z. Li, H. Zhao, Vitamin B12/carbon nanotubes composites for highly efficient CO_2 electroreduction with in situ shell-isolated nanoparticle-enhanced Raman spectroscopy, Electrochim. Acta 466 (2023) 143024.
[31] A. Zhanaidarova, S.C. Jones, E. Despagnet-Ayoub, B.R. Pimentel, C.P. Kubiak, Re(tBu-bpy)(CO)3Cl supported on multi-walled carbon nanotubes selectively reduces CO_2 in water, J. Am. Chem. Soc. 141 (2019) 17270–17277.
[32] M. Cong, X. Chen, K. Xia, X. Ding, L. Zhang, Y. Jin, Y. Gao, L. Zhang, Selective nitrogen reduction to ammonia on iron porphyrin-based single-site metal–organic frameworks, J. Mater. Chem. A 9 (2021) 4673–4678.
[33] Y. Liu, X. Tu, X. Wei, D. Wang, X. Zhang, W. Chen, C. Chen, S. Wang, C-bound or O-bound surface: which one boosts electrocatalytic urea synthesis? Angew. Chem., Int. Ed. 62 (2023) e202300387.
[34] F. Xu, X. Liu, L. Zhang, M. Guo, M. Li, X. Ding, L. Zhang, Revealing and optimizing the dialectical relationship between NOR and OER: cation vacancy engineering enables RuO2 with unanticipated high electrochemical nitrogen oxidation performance, Adv. Energy Mater. 13 (2023).
[35] X. Zhang, X. Zhu, S. Bo, C. Chen, M. Qiu, X. Wei, N. He, C. Xie, W. Chen, J. Zheng, P. Chen, S.P. Jiang, Y. Li, Q. Liu, S. Wang, Identifying and tailoring C–N coupling site for efficient urea synthesis over diatomic Fe–Ni catalyst, Nat. Commun. 13 (2022) 5337.
[36] C. Lv, L. Zhong, H. Liu, Z. Fang, C. Yan, M. Chen, Y. Kong, C. Lee, D. Liu, S. Li, J. Liu, L. Song, G. Chen, Q. Yan, G. Yu, Selective electrocatalytic synthesis of urea with nitrate and carbon dioxide, Nat. Sustain. 4 (2021) 868–876.
[37] G. Kresse, J. Furthmüller, Efficiency of ab-initio total energy calculations for metals and semiconductors using a plane-wave basis set, Comput. Mater. Sci. 6 (1996) 15–50.
[38] G. Kresse, J. Furthmüller, Efficient iterative schemes for ab initio total-energy calculations using a plane-wave basis set, Phys. Rev. B 54 (1996) 11169–11186.
[39] J.P. Perdew, K. Burke, M. Ernzerhof, Generalized gradient approximation made simple, Phys. Rev. Lett. 77 (1996) 3865–3868.
[40] S. Grimme, Semiempirical GGA-type density functional constructed with a long-range dispersion correction, J. Comput. Chem. 27 (2006) 1787–1799.
[41] A. Maurin, M. Robert, Noncovalent Immobilization of a Molecular Iron-Based Electrocatalyst on Carbon Electrodes for Selective, Efficient CO2-to-CO Conversion in Water, J. Am. Chem. Soc. 138 (2016) 2492–2495.
[42] T. Yao, L.-H. Zhang, J. Zhan, Z. Zhou, Y. You, Z. Zhang, F. Yu, Enhanced electrochemical CO2reduction performance of cobalt phthalocyanine with precise regulation of electronic states, Chem. Commun. 59 (2023) 7807–7810.
[43] W. Zhang, E.J. Meeus, L. Wang, L.H. Zhang, S. Yang, B. de Bruin, J.N.H. Reek, F. Yu, Boosting electrochemical oxygen reduction performance of iron phthalocyanine through axial coordination sphere interaction, ChemSusChem 15 (2022).
[44] M.X. Guo, L. Fang, L.L. Zhang, M.Z. Li, M.Y. Cong, X.P. Guan, C.W. Shi, C.L. Gu, X. Liu, Y. Wang, X. Ding, Pulsed electrocatalysis enabling high overall nitrogen fixation performance for atomically dispersed Fe on TiO, Angew. Chem., Int. Ed. 62 (2023) e202217635.
[45] E.M. Scheuring, W. Clavin, M.D. Wirt, L.M. Miller, R.F. Fischetti, Y. Lu, N. Mahoney, A. Xie, J.-j Wu, M.R. Chance, Time-resolved X-ray absorption spectroscopy of photoreduced base-off Cob(II)alamin compared to the Co(II) species in clostridium thermoaceticum, J. Phys. Chem. 100 (1996) 3344–3348.
[46] I. Sagi, M.R. Chance, Extent of trans effects in (nonalkyl)cobalamins: steric effects control the cobalt-nitrogen distance to 5,6-dimethylbenzimidazole, J. Am. Chem. Soc. 114 (1992) 8061–8066.
[47] Z. Miao, J. Meng, M. Liang, Z. Li, Y. Zhao, F. Wang, L. Xu, J. Mu, S. Zhuo, J. Zhou, In-situ CVD synthesis of Ni@N-CNTs/carbon paper electrode for electro-reduction of CO_2, Carbon 172 (2021) 324–333.
[48] S. Deng, P. Yuan, X. Ji, D. Shan, X. Zhang, Carbon nitride nanosheet-supported porphyrin: a new biomimetic catalyst for highly efficient bioanalysis, ACS Appl. Mater. Interfaces 7 (2014) 543–552.
[49] Y. Huang, Y. Wang, Y. Liu, A. Ma, J. Gui, C. Zhang, Y. Yu, B. Zhang, Unveiling the quantification minefield in electrocatalytic urea synthesis, Chem. Eng. J. 453 (2023) 139836.
[50] Z. Nie, L. Zhang, X. Ding, M. Cong, F. Xu, L. Ma, M. Guo, M. Li, L. Zhang, Catalytic kinetics regulation for enhanced electrochemical nitrogen oxidation by Ru-nanoclusters-coupled Mn3O4 catalysts decorated with atomically dispersed Ru atoms, Adv. Mater. 34 (2022) 2108180.
[51] D. Yue, Y. Jia, Y. Yao, J. Sun, Y. Jing, Structure and electrochemical behavior of ionic liquid analogue based on choline chloride and urea, Electrochim. Acta 65 (2012) 30–36.
[52] R. Keuleers, H.O. Desseyn, B. Rousseau, C. Van, Alsenoy, vibrational analysis of urea, J. Phys. Chem. A 103 (1999) 4621–4630.
[53] M.R. Manivannan, S. Investigation, of inhibitive action of urea-Zn^{2+} system in the corrosion control of carbon steel in sea water, Int. J. Eng. Sci. Technol. 3 (2011) 8048–8060.